THE JOURNAL OF BIOLOGICAL CHEMISTRY VOL. 285, NO. 52, pp. 40891–40900, December 24, 2010

NMR-derived Topology of a GFP-photoprotein Energy Transfer Complex*[S]

Received for publication, April 15, 2010, and in revised form, August 30, 2010 Published, JBC Papers in Press, October 6, 2010, DOI 10.1074/jbc.M110.133843

Maxim S. Titushin[‡§1], Yingang Feng (冯银刚)[‡1], Galina A. Stepanyuk[§¶], Yang Li (李杨)[‡], Svetlana V. Markova[§], Stefan Golz[‖], Bi-Cheng Wang (汪必诚)[¶], John Lee[¶], Jinfeng Wang (王金凤)[‡], Eugene S. Vysotski[§], and Zhi-Jie Liu (刘志杰)[‡2]

From the [‡]National Laboratory of Biomacromolecules, Institute of Biophysics Chinese Academy of Sciences, Datun Road 15, Beijing 100101, China, the [§]Laboratory of Photobiology, Institute of Biophysics Russian Academy of Sciences, Siberian Branch, Krasnoyarsk 660036, Russia, the [‖]Bayer Schering Pharma AG, BSP-GDD-GTR-TD-GT, Wuppertal 42096, Germany, and the [¶]Department of Biochemistry and Molecular Biology, University of Georgia, Athens, Georgia 30602

Förster resonance energy transfer within a protein-protein complex has previously been invoked to explain emission spectral modulation observed in several bioluminescence systems. Here we present a spatial structure of a complex of the Ca^{2+}-regulated photoprotein clytin with its green-fluorescent protein (*cg*GFP) from the jellyfish *Clytia gregaria*, and show that it accounts for the bioluminescence properties of this system *in vitro*. We adopted an indirect approach of combining x-ray crystallography determined structures of the separate proteins, NMR spectroscopy, computational docking, and mutagenesis. Heteronuclear NMR spectroscopy using variously ^{15}N,^{13}C,^{2}H-enriched proteins enabled assignment of backbone resonances of more than 94% of the residues of both proteins. In a mixture of the two proteins at millimolar concentrations, complexation was inferred from perturbations of certain ^{1}H-^{15}N HSQC-resonances, which could be mapped to those residues involved at the interaction site. A docking computation using HADDOCK was employed constrained by the sites of interaction, to deduce an overall spatial structure of the complex. Contacts within the clytin-*cg*GFP complex and electrostatic complementarity of interaction surfaces argued for a weak protein-protein complex. A weak affinity was also observed by isothermal titration calorimetry (K_D = 0.9 mM). Mutation of clytin residues located at the interaction site reduced the degree of protein-protein association concomitant with a loss of effectiveness of *cg*GFP in color-shifting the bioluminescence. It is suggested that this clytin-*cg*GFP structure corresponds to the transient complex previously postulated to account for the energy transfer effect of GFP in the bioluminescence of aequorin or Renilla luciferase.

The bioluminescence of many marine coelenterates, well-studied examples being the jellyfish *Aequorea* and the sea-pansy *Renilla*, involves the interaction of two proteins, a Ca^{2+}-regulated photoprotein in the jellyfish case, aequorin, and its cognate green-fluorescent protein, Aequorea GFP (1). Addition of Ca^{2+} to the purified aequorin produces a blue bioluminescence. It was early recognized that, in the jellyfish itself, the *in vivo* bioluminescence was a green color and after further study, the origin of this green emission was identified as the GFP. A Förster-type resonance energy transfer (FRET)[3] mechanism was invoked to explain how this bioluminescence spectrum is shifted (2). However, the well-known Förster theory requires concentrations of the donor-acceptor partners in the millimolar range, whereas in some bioluminescence systems, *e.g.* from the sea pansy *Renilla* and also the jellyfish *Clytia* subject herein, the GFP effect on the *in vitro* bioluminescence is observed at micromolar concentrations (3). Clearly the bioluminescence interaction has to involve formation of a complex and, in the case of *Renilla*, the formation of a luciferase-GFP complex has been shown (3).

In this work, we have determined by x-ray crystallography the spatial structures of the recombinant Ca^{2+}-regulated photoprotein clytin and Clytia GFP (*cg*GFP), which were cloned from a single specimen of *Clytia gregaria* (syn. *Phialidium gregarium*). Based on the structures, NMR titration experiments were employed to identify the interaction surfaces in a complex of both proteins. For a mixture of clytin and *cg*GFP at millimolar concentration, ^{1}H-^{15}N HSQC experiments revealed perturbation of chemical shifts of the separate proteins, which could be mapped to particular residues being affected by complexation. The NMR experiments also indicated that the association was weak but from knowledge of the interaction surface, computational docking was employed

* This work was supported by the National Natural Science Foundation of China, Ministry of Science and Technology of China, CAS Research Grant, CAS Fellowship for Young International Scientists Grant, Russian Foundation for Basic Research (08-09-92209 RFBR-China joint grant), SB RAS Grant 2, "Molecular and Cell Biology" program of RAS, Bayer AG (Germany), and by the University of Georgia Research Foundation and the Georgia Research Alliance.

The atomic coordinates and structure factors (codes 3KPX and 2HPW) have been deposited in the Protein Data Bank, Research Collaboratory for Structural Bioinformatics, Rutgers University, New Brunswick, NJ (http://www.rcsb.org/).

The backbone resonance assignments of clytin and cgGFP are available at the Biological Magnetic Resonance Data Bank with accession codes BMRB 16599 for clytin and BMRB 16600 for cgGFP.

[S] The on-line version of this article (available at http://www.jbc.org) contains supplemental Figs. S1–S5 and PDB data.

[1] Both authors contributed equally to this work.

[2] To whom correspondence should be addressed: Datun Road 15, Beijing 100101, China. Fax: 86-10-64888426; E-mail: zjliu@ibp.ac.cn.

[3] The abbreviations used are: FRET, Förster resonance energy transfer; *cg*GFP, green-fluorescent protein from jellyfish *C. gregaria*; HSQC, heteronuclear single quantum coherence spectroscopy; ITC, isothermal titration calorimetry; RMSD, root mean square deviation; AIR, ambiguous interaction restraint.

to propose an overall three-dimensional structure of the clytin-*cg*GFP complex.

EXPERIMENTAL PROCEDURES

Molecular Biology—Cloning of the clytin and Clytia GFP genes from a single specimen of the jellyfish *C. gregaria,* expression, purification, and characterization of recombinant clytin and *cg*GFP have been published (4). Site-directed and truncation mutagenesis of clytin were done on the template p22-Cl3 *E. coli* expression plasmid carrying the apo-clytin gene of wild-type *C. gregaria*. Mutations resulting in the amino acid change: K11A, K13A, N15A, N109A, or N188A were carried out using the QuickChange site-directed mutagenesis kit (Stratagene). N-terminal-truncated clytin mutants 5A (sequence starts from Ala-5) and 10V were amplified by PCR. The plasmids harboring mutations were verified by DNA sequencing.

Crystallography—Crystals of clytin grew at 16 °C within 1 week to a size of 50 × 50 × 300 μm. The crystallization droplet was set up using Mosquito crystallization robot (TTP Labtech) and contained equal volumes of protein (15 mg/ml) and reservoir solution (20% PEG-3350, 0.2 M NaH_2PO_4, pH 8.8) derived from the Peg/Ion crystallization screen (Hampton Research). The crystal was flash-frozen in liquid nitrogen. Native diffraction data were indexed and scaled to 1.9 Å resolution using HKL2000. The space group of clytin was $C222_1$ with unit cell dimensions (Å), a = 43.39, b = 68.93, c = 115.35. Phases were determined by molecular replacement with PHASER (5), using the structure of obelin (PDB code 1JFO) as a search model. The final models were refined with PHENIX (6). Manual adjustments to the model were done using COOT (7). The quality of the final model was validated with MOLPROBITY (8). The detailed data processing and refinement statistics are shown in Table 1.

Crystals of *cg*GFP grew at 4 °C within 5 days to a size of 200 × 200 × 250 μm. The crystallization droplet contained equal volumes of protein (9 mg/ml) and reservoir solution (2 M ammonium sulfate, 0.1 M sodium citrate, pH 5.5) derived from the Wizard I crystallization screen (Emerald Biosystems). The crystal was flash-frozen in liquid nitrogen. Native diffraction data were indexed and scaled to 1.55 Å resolution using HKL2000. The space group of *cg*GFP was $I2_12_12_1$ with unit cell dimensions (Å), a = 53.09, b = 91.45, c = 110.61. Phases were determined by molecular replacement with MOLREP (9) using GFP from *Aequorea victoria* as a search model (PDB code 1EMA). Iterative model validation, rebuilding and refinement, were carried out with MOLPROBITY (8), XFIT (10), and REFMAC5 (11), respectively. The detailed data processing and refinement statistics on *cg*GFP are shown in Table 1.

Protein concentrations were determined by the dye-binding method of Bradford (12) using an assay kit (Bio-Rad) and bovine serum albumin as a standard. On this basis extinction coefficients for clytin (ϵ_{280} = 65,200 M^{-1} cm^{-1}) and *cg*GFP (ϵ_{485} = 64,000 M^{-1} cm^{-1}) were calculated and subsequently, protein concentrations were determined by absorbance.

NMR Sample Preparation—Uniformly ^{15}N- or ^{15}N-, ^{13}C-labeled clytin and *cg*GFP were obtained from the cells grown in M9 minimal medium containing $^{15}NH_4Cl$ or additional [^{13}C]glucose. To acquire ^{15}N-, ^{13}C-, and 60% ^{2}H-labeled *cg*GFP, 99.8% $^{2}H_2O$-based M9 was used. To exchange amide group deuterium to hydrogen, triple-labeled *cg*GFP was subjected to reversible denaturation in 6 M guanidine-HCl for 10 min, followed by 20-fold droplet dilution in PBS at 25 °C and overnight incubation at 4 °C. Activity of *cg*GFP was restored upon refolding as indicated by absorbance and fluorescence spectra and bioluminescence color shift assay with clytin.

NMR Spectroscopy—NMR experiments were performed on Bruker DMX 600 MHz and Avance 800 MHz spectrometers equipped with z-gradient triple-resonance cryo-probes. Data were processed in FELIX (Accelrys Inc.) and visualized with NMRVIEW (13). The backbone assignments were obtained by MARS (14). All NMR samples were dissolved in buffer containing 20 mM Tris-HCl, pH 7.0, 10 mM NaCl, 2 mM EDTA, 0.01% (w/v) sodium 2,2-dimethylsilapentane-5-sulfonate (DSS) and 10% (v/v) $^{2}H_2O$. The experiments for the backbone assignments of clytin include two-dimensional ^{1}H-^{15}N HSQC, and 3D ^{1}H-^{15}N-^{13}C HNCA, HNCACB, CBCA-(CO)NH, HNCO, HN(CA)CO, HBHA(CBCA)NH, HB-HA(CBCA)(CO)NH (15), all performed at 293 K. The experiments for the backbone assignments of *cg*GFP include deuterium-decoupled 3D HNCACB, CBCA(CO)NH, HNCO, HN(CA)CO using ^{15}N-, ^{13}C-, and 60% ^{2}H-labeled *cg*GFP sample and 4D ^{13}C,^{15}N-edited NOESY (16) using ^{15}N-, ^{13}C-labeled *cg*GFP sample, all performed at 310 K. The backbone assignments for GFP at 298 K were obtained from those at 310 K by following the shift of resonance signals in a series of two-dimensional ^{1}H-^{15}N HSQC spectra recorded at decreasing temperatures.

Chemical shift perturbation analyses were performed at 293 K for clytin and 298 K for *cg*GFP by monitoring the two-dimensional ^{1}H-^{15}N HSQC spectra of titrated proteins. Unlabeled clytin WT or mutants K11A, K13A, N109A, N188A, and 5A (0.5 mM, 1 mM), were added to ^{15}N- or ^{15}N-, ^{2}H-labeled *cg*GFP (0.4 mM). Alternatively, unlabeled *cg*GFP (0.3 mM, 0.6 mM) was added to ^{15}N-labeled clytin (0.2 mM). The amide hydrogen and nitrogen chemical shift changes were calculated according to Equation 1,

$$CSP = \mathrm{sqrt}(\Delta\delta_H^2 + 0.2\Delta\delta_N^2) \quad \text{(Eq. 1)}$$

where $\Delta\delta_N$ and $\Delta\delta_H$ represent the changes in the amide nitrogen and proton chemical shifts (in parts per million), respectively.

Calculations of the Clytin-cgGFP Complex Structure—The computational structures of the clytin-*cg*GFP complex were generated with HADDOCK2.0 (17, 18) in combination with CNS (19). Ambiguous interaction restraints (AIRs) were generated for both clytin and *cg*GFP based on chemical shift perturbation studies (Table 2) as described (17). The starting structures were the monomer *cg*GFP (PDB code 2HPW) and the clytin (PDB code 3KPX) with the manually added 2–8 N-terminal segment, which is absent in the deposited structure and was defined as fully flexible during docking. The standard HADDOCK protocol was used. For the rigid-body energy minimization, 1,000 structures were generated, with

the 200 lowest energy solutions used for subsequent semi-flexible simulated annealing and water refinement. Resulting structures were sorted according to intermolecular energy and clustered using a 7.5 Å cut-off criterion. Subsequent cluster analysis was performed within a 4.0 Å cut-off criterion. The 10 lowest energy solutions were taken to represent the structure of the complex (supplemental PDB files).

Bioluminescence Assay—Bioluminescence spectra of clytin and clytin with *cg*GFP, were measured with a Varioskan Flash Spectrofluorimeter (Thermo Scientific). All measurements were carried out at 25 °C. Luminescence was triggered by injection of 7 μl of 40 mM $CaCl_2$ into the wells containing 150 μl of isolated clytin (final concentration is in the 0.4–1.5 μM range) or clytin mixed with *cg*GFP (final concentrations from 0 to 9.7 μM) in 2 mM EDTA, 10 mM NaCl, 20 mM Tris-HCl, pH 7.0 buffer. Emission spectra were fully corrected for instrumental spectral sensitivity with the computer program supplied with the instrument, and also for bioluminescence intensity decay over the time for the spectral scan. All spectra were the average of three measurements. The energy transfer efficiency coefficient (K_{ET}) for clytin and clytin mutants was determined by plotting the I_{500}/I_{470} ratio *versus* total concentration of *cg*GFP, where I_{500} and I_{470} are bioluminescence intensities at 500 nm and 470 nm, respectively. The slope of the linear regression fitted data was taken as the K_{ET} value.

Isothermal Titration Calorimetry—Isothermal titration calorimetry measurements were performed on an ITC_{200} calorimeter (Microcal Inc., Northampton, MA). All experiments were carried out at 25 °C in 20 mM Tris-HCl, 10 mM NaCl, 2 mM EDTA, pH 7.0. The reactant (0.1 mM clytin) was placed in the 200-μl sample chamber and *cg*GFP (4.68 mM for monomer) in the syringe was added with 20 successive additions of 2 μl for 4 s (with an initial injection of 0.5 μl). The interval between each injection lasted 150 s. The peaks generated were corrected for *cg*GFP heat of dilution and integrated using the ORIGIN software (Microcal Inc) by plotting the values in microcalories against the ratio of total moles of injectant, monomer *cg*GFP, to reactant clytin, within the cell. Data were fit using a 1:1 clytin:*cg*GFP monomer binding model.

TABLE 1

X-ray structure statistics

	clytin	*cg*GFP
Data collection		
Resolution range (Å)	50–1.9 (2.0–1.9)[a]	27.7–1.47 (1.52–1.47)
Wavelength (Å)	1.54	0.979
Space group	$C222_1$	$I2_12_12_1$
Cell dimensions		
a, *b*, *c* (Å)	43.39, 68.93, 115.35	53.09, 91.45, 110.61
α, β, γ (°)	90, 90, 90	90, 90, 90
Unique reflections	14018 (1326)	40289 (3811)
Completeness (%)	99.5 (95.9)	86.7 (20.3)
$I/\sigma(I)$	26.43 (2.82)	38.77 (2.25)
R_{sym} (%)	11.2 (60.5)	4.9 (14.5)
Redundancy	13.0 (6.4)	4.4 (1.5)
Refinement		
Resolution range (Å)	50–1.9	10–1.55
Reflections used	13990 (728)	36117 (1877)
R_{work}, R_{free}	17.07%, 21.94%	18.2%, 20.2%
Mean B factor (Å^2)	19.12	14.27
Protein atoms	1678	1827
Solvent atoms	128	235
RMSD bond lengths (Å)	0.011	0.015
RMSD angles (°)	1.185	1.407

[a] Values for the highest resolution shell are given in parentheses.

RESULTS

Crystal Structures of Clytin and cgGFP—Both proteins were separately crystallized and their structures determined by x-ray crystallography (Table 1). Clytin has molecular mass of 22.4 kDa and shares high structural and sequence similarity with the other Ca^{2+}-regulated photoproteins, obelin (20) (RMSD 0.66 Å, sequence identity 74%) and aequorin (21) (RMSD 1.39 Å, sequence identity 57%) (Fig. 1*A*). All have four helix-loop-helix motives, three EF-hand Ca^{2+}-binding loops, and the substrate 2-hydroperoxycoelenterazine bound in a hydrophobic cavity (22) (Fig. 2*A*). Additionally, a contaminant metal ion is found within EF-hand I loop, which approaches the non-standard conformation similar to EF-hand I of obelin, whose crystal was briefly soaked with Ca^{2+} (23). There is

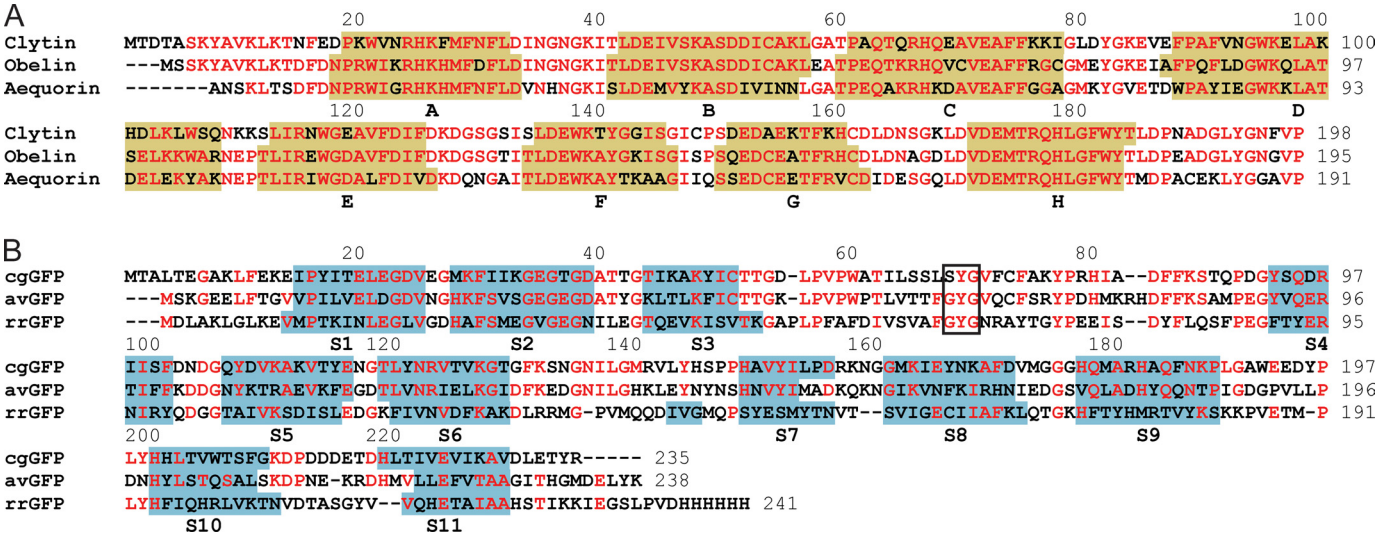

FIGURE 1. **Protein sequence alignments of (*A*) photoproteins: clytin, obelin (PDB code 1QVO) and aequorin (PDB code 1EJ3); and (*B*) GFPs: *cg*GFP, Aequorea GFP (*av*GFP) (PDB code 1EMA) and Renilla GFP (*rr*GFP) (PDB code 2HR7).** Identical residues are *red*. Secondary structure elements are highlighted in *yellow* (α helices A–H of photoproteins) and *light blue* (β strands S1–S11 of GFPs). Residues comprising the chromophore of GFPs are enclosed in *black box*.

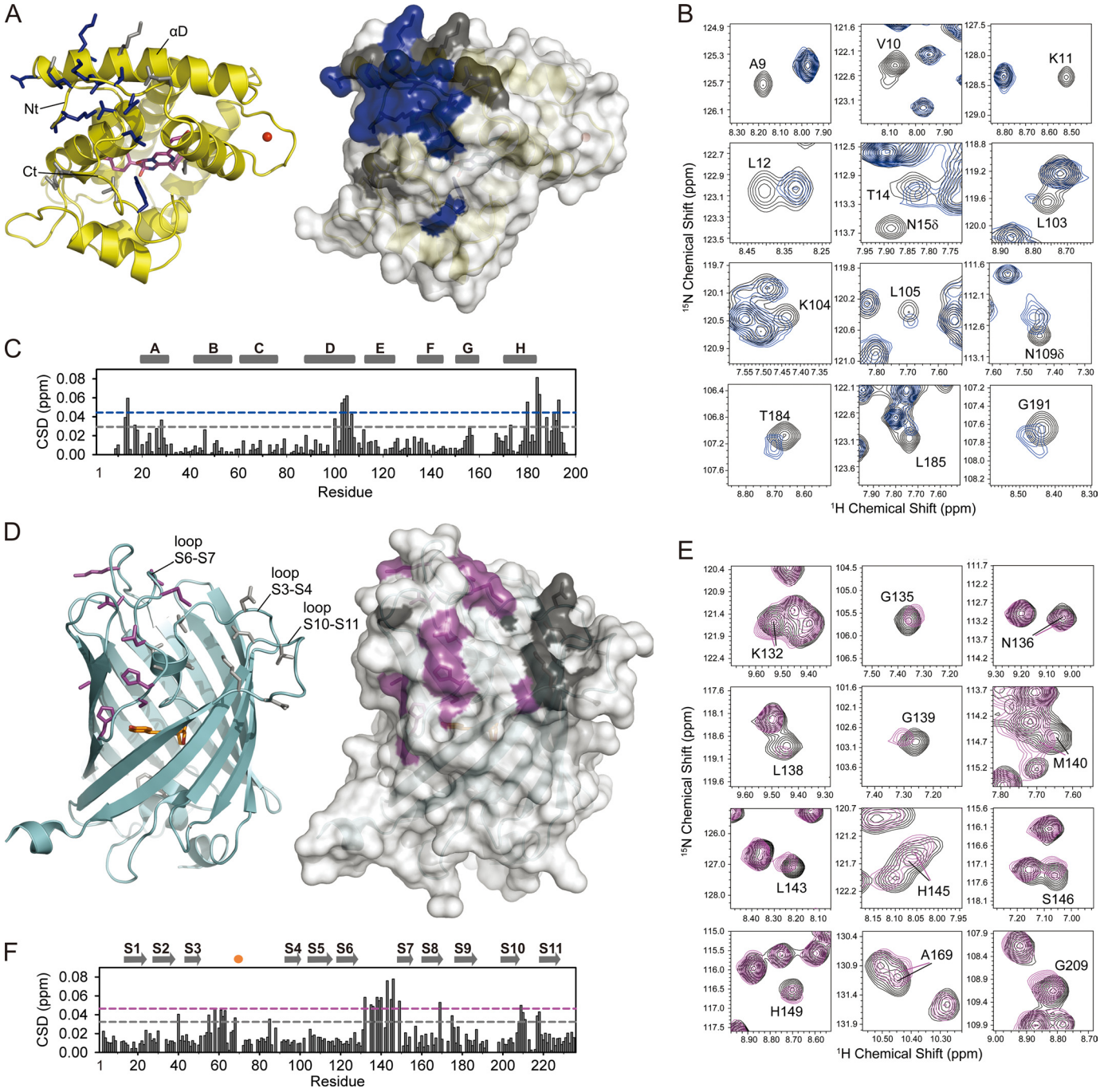

FIGURE 2. **Chemical shift mapping identifies the interaction surfaces of clytin and *cg*GFP.** On crystal structures of clytin (*A*) and *cg*GFP (*D*) the interfacial residues mapped according to cross-peak/intensity shift are shown as sticks and highlighted in color on the surface. *B* & *E*, ^{1}H-^{15}N HSQC spectra areas derived from superposition of ^{15}N-labeled clytin (*B*, *black*) and ^{15}N, ^{2}H-labeled *cg*GFP (*E*, *black*) with unlabeled *cg*GFP (*blue*) and clytin (*magenta*), respectively. *C* & *F*, weighted-average chemical shift differences (*CSD*) between ^{15}N-clytin (*C*) or ^{15}N,^{2}H-*cg*GFP (*F*) and 1:3 ^{15}N-clytin/*cg*GFP and 1:2 ^{15}N,^{2}H-*cg*GFP/clytin mixtures. The *dashed lines* represent the one standard deviation (*gray*) and two standard deviations (*blue, magenta*) cut-offs. Residues, whose cross-peak shifted more than one or two standard deviations above the average, are mapped on the spatial structures in *gray* and *blue* for clytin, and in *gray* and *magenta* for *cg*GFP, respectively. Residues of clytin (mostly N-terminal) with significant peak intensity perturbations, are also mapped in *blue*.

no electron density for the Thr^{2}-Ala^{9} region implying significant structural flexibility of the N terminus of clytin. *cg*GFP forms the well-known barrel structure built of 11 β strands (S1–S11) with the chromophore buried inside (24, 25) (Fig. 2*B*). Despite a low sequence identity (Fig. 1*B*), the structure of *cg*GFP highly resembles GFPs from *Aequorea* (26) (RMSD 1.04 Å, sequence identity 41%), and *Renilla* (27) (RMSD 1.84 Å, sequence identity 19%). The *cg*GFP homodimer can be generated from the *cg*GFP monomer in the crystallographic asymmetric unit by applying a 2-fold symmetry axis. The dimerized form of *cg*GFP is evident from a mass of 52 kDa determined by analytical ultracentrifugation, close to that of the natural *cg*GFP (57 kDa) (28, 29), consistent with the 27 kDa monomer mass determined by SDS-PAGE. The *cg*GFP monomer buries 1,370 Å^{2} (13% of the total surface area) in the dimer interface.

Mapping the Clytin-cgGFP Interface—The backbone NMR resonance assignments of both proteins, which are the basis for our chemical shift perturbation mapping, were obtained by heteronuclear NMR spectroscopy using $^{15}N,^{13}C$-labeled clytin and $^{15}N,^{13}C,^{2}H$-labeled *cg*GFP. The backbone resonances of more than 94% residues were assigned for both proteins (supplemental Fig. S1). Lack of assignment for residues Lys^{159}–Asn^{165} located at the end of α-helix G and the EF-hand IV loop of clytin might be due to the line broadening caused by the structural flexibility in this region.

A similar effect was shown in the NMR study of aequorin (30). Line broadening for the Thr^{2}–Lys^{7} residues of clytin is in agreement with x-ray crystallography verified structural flexibility of the N terminus. Residues of *cg*GFP lacking assignments mostly belong to the loop regions comprising the top and bottom of the GFP barrel.

We were unable to crystallize any clytin-*cg*GFP complex either from a mixture of proteins or for a covalently cross-linked complex under around 300 crystallization conditions available from commercial kits (Hampton Research, Emerald Biosystems). Instead evidence for protein-protein association was inferred from two ^{1}H-^{15}N HSQC titration experiments, first with ^{15}N-labeled clytin and unlabeled *cg*GFP, then *vice versa*. NMR titration could not be saturated because of the limited solubility of both proteins and the weak interaction between them, and therefore the K_{eq} could not be derived from the NMR titration data (supplemental Fig. S5). Protein concentrations were 0.3–1 mM, which implies an equilibrium constant K_{eq} in the mM range. Nevertheless, a number of peaks in the HSQC spectra showed chemical shift and/or peak intensity perturbations from which the binding surfaces of clytin and cgGFP were mapped (31–34) (Fig. 2). The perturbed peaks show concentration-dependent chemical shift changes, which indicates a fast exchange on the NMR chemical shift time scale (supplemental Fig. S5).

When mapping the perturbed residues on the structures of clytin and *cg*GFP, these residues are well clustered on the surfaces of both proteins, which implies specific interactions between the two proteins (Fig. 2). The remaining chemical shift changes upon the titration are relatively small (Fig. 2, *C* & *F*), with maximum chemical shift perturbation values for both proteins not exceeding 0.08 ppm, which indicates no large structural rearrangement during the complex formation. For clytin (Fig. 2, *B* & *C*), the perturbations are assigned to residues within three segments: 9–17 at the N terminus, 100–109 in the α-helix D, and at the C terminus, 180–193, as well as some adjacent residues. For *cg*GFP (Fig. 2, *E* & *F*), the perturbations are identified as belonging to residues 55–65, mainly in segments of loop S3–S4 and the central α-helix, 132–149 of the longest loop S6–S7 covering the GFP barrel from the top, and 209–218 of the remarkably acidic loop S10–S11, as well as some adjacent residues. For *cg*GFP, however, chemical shifts are also detected for residues buried inside the protein molecule. These are segment 60–66, "connecting" the interaction surface with the chromophore, and Ser^{146} and His^{149}, which form hydrogen bonds with Tyr^{69} of the chromophore through the water molecule. The *cg*GFP contact surface is less uniform and narrower than that of clytin, which may be explained by overlapping or lack of assignment for some of the resonances in the main interacting regions: excluding prolines these are Ser^{133}, Asn^{134}, Ile^{137}, Arg^{141}, Tyr^{144} of the loop S6–S7 and Asp^{215} of the loop S10–S11. On the clytin-*cg*GFP complex structure these residues are found buried in the protein-protein contact region. *cg*GFP forms a homodimer in solution, and there is no overlap between the *cg*GFP dimer interface and the clytin-binding patches.

TABLE 2
List of active and passive residues of clytin and *cg*GFP derived from chemical shift perturbation plots, which comprised AIRs for HADDOCK docking

	Active	Passive
clytin	Ala^{5}, Ala^{9}, Val^{10}, Leu^{12}, Lys^{13}, Thr^{14}, Asn^{15}, Glu^{17}, Lys^{100}, Lys^{104}, Ser^{107}, Asn^{109}, Asn^{188}, Gly^{191}	Thr^{2}, Glu^{3}, Thr^{4}, Ser^{6}, Lys^{7}, Tyr^{8}, Lys^{11}, Pro^{19}, Glu^{97}, Asn^{108}, Lys^{110}, His^{160}, Pro^{187}
***cg*GFP**	Glu^{55}, Lys^{132}, Leu^{138}, Met^{140}, Leu^{143}, His^{145}, Gly^{175}, Gly^{209}, Lys^{210}	Gly^{54}, Asn^{103}, Asp^{104}, Gly^{130}, Phe^{131}, Ser^{133}, Asn^{134}, Met^{173}, Gly^{174}, Gly^{176}, Phe^{208}, Pro^{212}

We employed isothermal titration calorimetry (ITC) to obtain an independent assessment of the interaction of clytin with *cg*GFP. ITC has been shown to be capable of recovering weak binding constants although the accuracy of thermodynamic parameters is problematic compared with protein-protein affinities in the micromolar regime (57). The net heats of interaction of *cg*GFP as titrant added to clytin are shown in Fig. 7. The experiment and data analysis take into account the precautions suggested by Turnbull *et al.* (57). Above molar ratio about 3.0 there is large uncertainty due to the mixing signal being hardly different from the control dilution heat of *cg*GFP alone. The full line is an unweighted fit to a binding model with fixed stoichiometry ($n = 1.0$) using a 1 clytin:1 *cg*GFP monomer binding model, and the derived affinity constant is $K_D = 0.90 \pm 0.07$ mM. A model with 1 clytin:1 *cg*GFP dimer yields almost the same result. This affinity is consistent with the millimolar range estimate for K_{eq} from the NMR titration experiment. Interestingly, clytin and *cg*GFP could be separately concentrated up to 50 mg/ml and 160 mg/ml, respectively, while the mixture of proteins always showed precipitation at concentrations higher than 30 mg/ml under the same conditions. Because the clytin-*cg*GFP complex buries predominantly hydrophilic residues, (discussed below), the decreased solubility of the protein mixture is more evidence of complexation at these concentrations.

Computational Docking of the Clytin-cgGFP Complex—Because of weak interaction between clytin and *cg*GFP under NMR conditions accompanied by the large molecular size of the proteins, it was not possible to derive accurate spatial restraints from measuring intermolecular NOEs for the complex. Therefore we use a docking approach, named HADDOCK2.0 (17, 18), which relies on ambiguous restraints originating from initial NMR chemical shift perturbation data (Table 2) to derive an accurate model of a protein-protein complex (31, 35–37). A feature of HADDOCK to introduce backbone flexibility was applied to the Thr^{2}-Ala^{9} N-terminal region of clytin. Fig. 3 is the computational result for the cly-

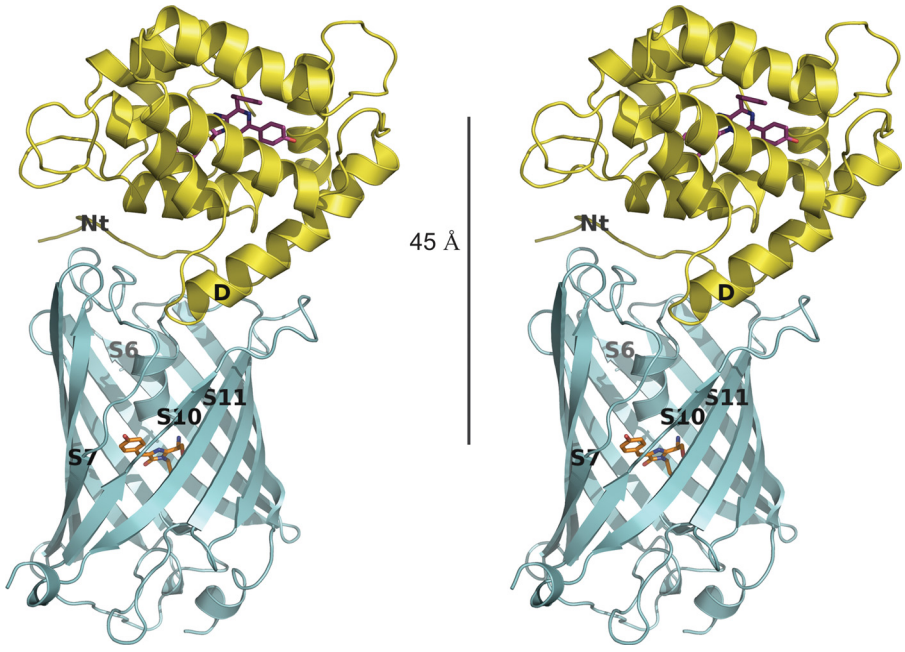

FIGURE 3. **Stereoview representation of the spatial structure of the clytin-*cg*GFP complex derived from x-ray structures of clytin and *cg*GFP, NMR-mapping of the interaction surfaces and computational docking in HADDOCK.** 45 Å is the distance between the two chromophores. Structural elements of clytin and *cg*GFP comprising the interaction surface are labeled.

tin-*cg*GFP complex dimer, initially based on the identified interaction surfaces which were highly suitable for structure calculation using HADDOCK. The family of final structures had the lowest intermolecular energy (−382.81 kcal/mol) and the highest buried surface area (1,913 Å^2) (supplemental Table S1). The average pairwise RMSD in this cluster is 1.29 ± 0.48 Å for backbone atoms. *cg*GFP forms a homodimer in solution, and the clytin-binding patch on each *cg*GFP monomer would be distant from each other, thus one *cg*GFP monomer could accommodate one clytin. As the HSQC chemical shift perturbations and the ITC data both indicate an interaction constant in the millimolar range, this is considered as very weak. The contact surface indeed reveals a relatively low number of hydrophobic contacts and hydrogen bonds, although in total the complex buries 1,913 ± 87 Å^2 of surface area, which is average for a protein-protein complex (38).

Calculation of the electrostatic potential of clytin and *cg*GFP reveals that the interfaces have remarkable charge complementarity, which might assist the complex stabilization (Fig. 4). The clytin α-helix D and the proximal N terminus carry the positive charge and occupy, also with good shape complementarity, the negatively charged gutter on the top of the *cg*GFP barrel formed by the S3–S4, the distal part of the S6–S7, and the S10–S11, loops. The S10–S11 loop is strongly acidic and appears as the least structured region of the *cg*GFP molecule. This may enable it to adjust for best fit to the clytin interface. In the 10 lowest free energy structures (supplemental Fig. S2 and PDB files), contacts in this region (Fig. 4) are prevalently formed by lysine residues of clytin (Lys^{11}, Leu^{12}, Lys^{13}, Thr^{14}, Lys^{100}, Lys^{104}) and aspartic and glutamic residues of *cg*GFP (Asp^{55}, Lys^{210}, Asp^{211}, Pro^{212}, Asp^{213}, Asp^{214}, Asp^{215}, Glu^{216}). Also Gln^{108} of clytin approaches Phe^{210} of *cg*GFP, and Asn^{109} of clytin lies adjacent to His^{145} and Tyr^{144} of *cg*GFP. As expected for electrostatic interactions, the clytin-*cg*GFP complex formation should be considerably sensitive to ionic strength (Fig. 6). These features of charge complementarity of interfaces together with a low binding affinity, are largely found among transient complexes of various proteins, the well studied examples being redox proteins and Ras or Rap with their signaling effectors (39–41).

Another major interacting region is moderately polar and comes from overlapping of the surface accessible region of the S6–S7 loop of *cg*GFP (residues Ser^{133}, Asn^{134}, Leu^{138}, Gly^{139}, Met^{140}, Arg^{141}) and some adjacent residues (Met^{173}, Met^{174}, Gly^{174}) by the distal part of the N terminus of clytin (Thr^2, Asp^3, Thr^4, Ala^5, Ser^6, Lys^7, Tyr^8, Ala^9, Val^{10}). The exact contacts in this region are highly variable because of flexibility of the residues 2–9 of clytin, which together with mutagenesis data discussed below implies a less important role for the N terminus of clytin in binding *cg*GFP compared with the charge complementarity region (Fig. 4). Superimposition of the 10 best structures of the complex demonstrates flexibility of structural elements comprising the interface (RMSD for Thr^2–Ala^9 region of clytin 4.51 ± 1.57 Å, RMSD for the S10–S11 loop of *cg*GFP 1.13 ± 0.21 Å) (supplemental Fig. S2).

Clytin Mutants—Site-directed and N-terminal truncation mutagenesis of clytin was introduced to assess the contribution of the residues found at the interface to the degree of protein association and to determine if there was a correlation with the effectiveness of *cg*GFP in producing the well-known bioluminescence color shift in the reaction. These mutants of clytin were K11A, K13A, N15A, N109A, N188A, and two N-terminal truncations (5A, 10V). All substitutions had negligible effect on the bioluminescence properties of clytin, implying no significant rearrangements in spatial structures of clytin mutants. Fig. 5 shows the bioluminescence spectral titration with *cg*GFP for one of the point mutants compared

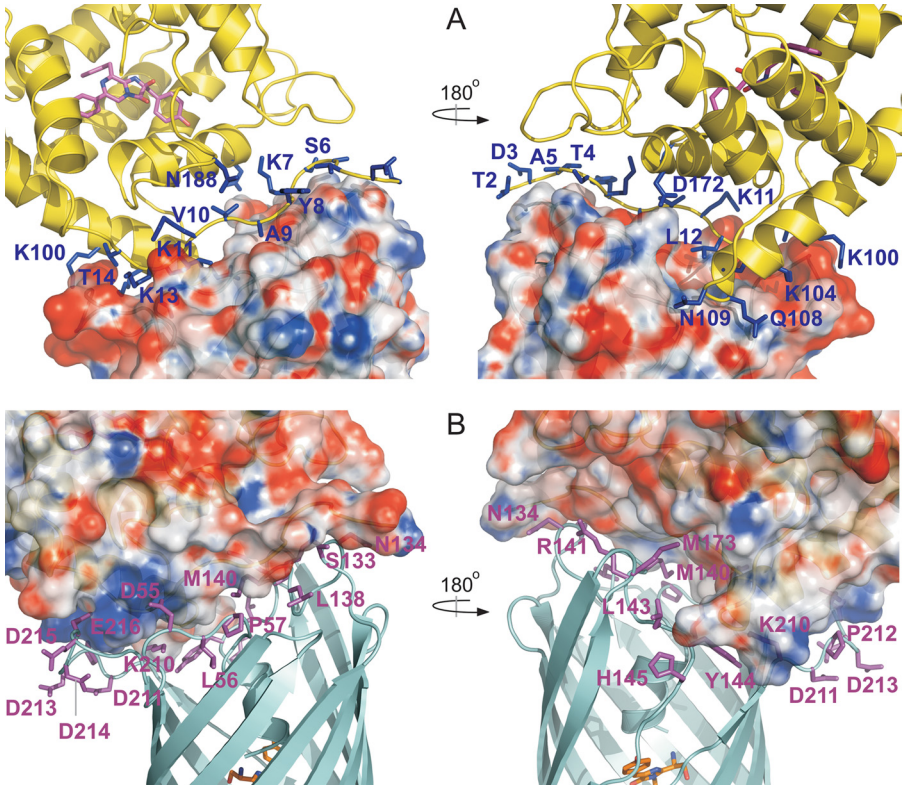

FIGURE 4. **The clytin-*cg*GFP interface.** Two views of the molecules are rotated by 180° to allow for viewing of the interaction surfaces. The electrostatic surface (−10*k*T/e–+10*k*T/e) of *cg*GFP (*A*) and clytin (*B*) are shown. Poisson-Boltzmann electrostatics calculations were done within PDB2PQR (55) and evaluated in APBS (56). The positively charged, negatively charged, and neutral amino acids are represented in *blue*, *red*, and *white*, respectively. Residues of clytin (*A*) and of *cg*GFP (*B*) buried in the contact surface are shown as *blue* and *magenta* sticks, respectively.

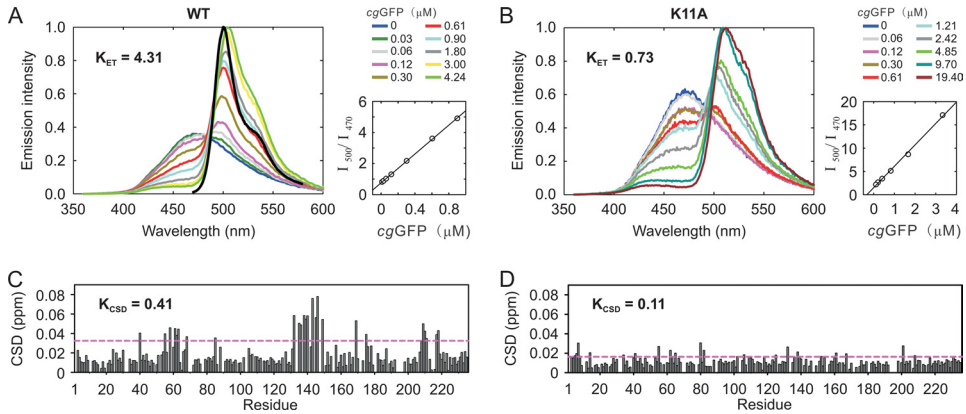

FIGURE 5. **Mutations of interfacial residues correspondingly decrease the affinity of the complex (K_{CSD}) together with the energy transfer efficiency (K_{ET}).** *A*, bioluminescence spectra of wild-type clytin (*left*) and K11A clytin (*right*) obtained upon titration with *cg*GFP (0–19.4 μM). The fluorescence spectrum of *cg*GFP is shown in *black* on the wild-type clytin spectrum (*left*). K_{ET} was determined from the corresponding plots as the slope of the I_{500}/I_{470} ratio *versus cg*GFP concentration, where I_{500} and I_{470} are bioluminescence intensities at 500 nm and 470 nm, respectively. *B*, weighted-average chemical shift differences (*CSD*) between $^{15}N,^{2}H$-*cg*GFP and mixtures of $^{15}N,^{2}H$-*cg*GFP with 1:2 molar excess of clytin (*left*), and K11A clytin (*right*), respectively. K_{CSD} was determined as a sum of CSD above the average CSD plus one standard deviation cut-off (*purple dashed line*) in ppm units.

with native clytin. The *cg*GFP effectiveness in producing a color shift was measured by an interaction constant, K_{ET}, and shown to decrease for all the mutants (supplemental Fig. S4) and most significantly for the substitution K11A (Fig. 5*A*). The degree of *cg*GFP HSQC chemical shift perturbations, obtained upon titration with clytin mutants, was used to calculate a quantitative parameter of protein association, named K_{CSD}. Values of chemical shift perturbation after subtracting the average perturbation plus one standard deviation were summed to give the K_{CSD} value in ppm units. Peak tables of *cg*GFP upon titration with clytin mutants are shown in supplemental Fig. S4 and for K11A mutant in Fig. 4*B*. The apparent association constant K_{CSD} correlates well with K_{ET}, all mutants show a decrease in K_{ET} with a lessening of the degree of association (K_{CSD}). Substitutions K11A, K13A, and the 10V truncation, had the strongest effect, reducing K_{ET} up to 4-fold from clytin along with a strong reduction in binding affinity. These positions are of interest because of their contribution to the surface charge complementarity of the interacting proteins. On the other hand it indicates the important role of the

charge complementarity region compared with the flexible N-terminal segment, because the effects of K11A and K13A substitutions are comparable to that of deleting the first 9 N-terminal residues of clytin. It also implies a minimal role of any small structural rearrangement of clytin mutants in affecting binding to *cg*GFP. Substitutions N109A, N15A, and N188A had strong, moderate and the smallest effect, respectively.

DISCUSSION

Energy transfer or the bioluminescence color shift on the addition of GFP, has previously received detailed study for two bioluminescence systems, that of aequorin and of Renilla luciferase (3, 42, 44–46). The mechanism has been proposed to be by FRET within a transient protein-protein complex. According to the well-known FRET equation, the probability or rate of energy transfer, from the excited donor to the acceptor, depends on several parameters, most critical being the donor-acceptor separation and the spectral overlap of donor fluorescence and acceptor absorption. A convenient measure is the "Förster separation" where the probability of the donor radiative $S_1 \rightarrow S_0$ transition equals the probability of energy transfer populating the acceptor S_1 state; in almost all cases this distance is less than 10 nm. This means that for the partners randomly distributed in free solution, they need to be in the millimolar concentration range. The bioluminescence color shifts however, are observed at micromolar protein concentrations so for FRET to be feasible the donor-acceptor separation must be constrained within a protein-protein complex.

For the Renilla luciferase bioluminescence in particular, the addition of Renilla GFP at micromolar concentrations, not only produced the green color shift but enhanced the bioluminescence quantum yield about three times. This is conclusive evidence for FRET indicating that efficient excited state coupling in the transient complex competes with both radiative and non-radiative deactivation pathways of the primary excited S_1 state formed by the reaction on the luciferase. A stable complex was not observed by direct methods, chromatography, fluorescence anisotropy, at these micromolar concentrations. However, using the Hummell-Dryer chromatographic method, Ward and Cormier (45) reported the presence of a Renilla luciferase-Renilla GFP complex. Further evidence that such a complex must be involved for the bioluminescence shift was that the energy transfer was specific for the type of GFP, it occurred with GFPs from other species of *Renilla* but not from GFPs of more distantly related organisms. Also, the shift effect was negated by amino acid modification in the GFP and by higher ionic strength in the buffer (>100 mM) (Fig. 6).

A complex has also been reported for the aequorin-Aequorea GFP bioluminescence using the Hummel-Dryer method (47). In that case no bioluminescence quantum yield increase accompanying the energy transfer was observed (42) as also the case here for the clytin bioluminescence in Fig. 5*A*. Morise *et al.* (42) however, demonstrated that energy transfer was significantly enhanced in a suspension of DEAE particles on which the aequorin and Aequorea GFP had been co-adsorbed, presumably bringing the two partners to proximity, but the color shift was also observed to an unrelated acceptor, FMN, meaning that it was nonspecific.

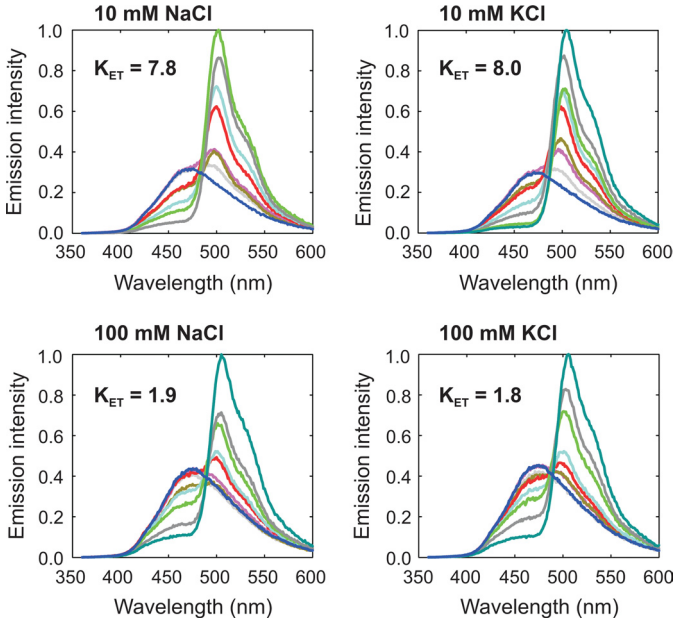

FIGURE 6. **Bioluminescence color-shift assay to show the ionic strength dependence of the clytin-*cg*GFP energy transfer measured as K_{ET}.** Bioluminescence spectra of clytin were obtained upon titration with *cg*GFP (0–3.62 μM; *dark blue line*, 0 μM; *gray line*, 0.03 μM; *purple line*, 0.06 μM; *dark yellow line*, 0.12 μM; *red line*, 0.24 μM; *light blue line*, 0.45 μM; *light green line*, 0.90 μM; *dark gray line*, 1.81 μM; *dark green line*, 3.62 μM). Concentration of clytin was 0.47 μM. Spectra were recorded in the buffer containing 20 mM PIPES, pH 7.2, 1 mM $MgCl_2$, 0.5 mM EDTA, and different concentrations of NaCl or KCl, upon injection of $CaCl_2$. Clytin and *cg*GFP were from a later batch, indicating some uncertainty in the absolute values of K_{ET} values.

The observations on the clytin bioluminescence system reported here bear similarity to these earlier reports. The clytin bioluminescence spectrum is shifted to the fluorescence of *cg*GFP by only micromolar concentrations of *cg*GFP, the effect is diminished by modification of amino acid residues in the clytin, which otherwise affect no change in the clytin bioluminescence properties, the *cg*GFP shift is an order of magnitude less effective using the distantly related photoprotein obelin, even though with this pair, the spectral overlap is significantly higher (4), and the K_{ET} is reduced but not eliminated at increased ionic strength.

Additional similarity to earlier reports was that no clytin-*cg*GFP interaction in the micromolar range could be detected by the methods of fluorescence anisotropy, analytical ultracentrifugation, or plasmon resonance (results not shown). However, in contrast to the cases of *Renilla* and aequorin just mentioned, Markova *et al.* (4) recently observed no complex by Hummel-Dryer chromatography using a starting concentration ten times higher than Ward and Cormier used for their *Renilla* experiment. Altogether, we estimate here a 0.9 mM value for the clytin-cgGFP affinity constant, consistent with the weak K_{eq} in the mM range inferred from the NMR perturbations.

Although the computational model in Fig. 3 needs to be interpreted with appropriate reservation, we point out that the spatial arrangement of the donor and acceptor makes it attractive to consider this complex as the functional biolumi-

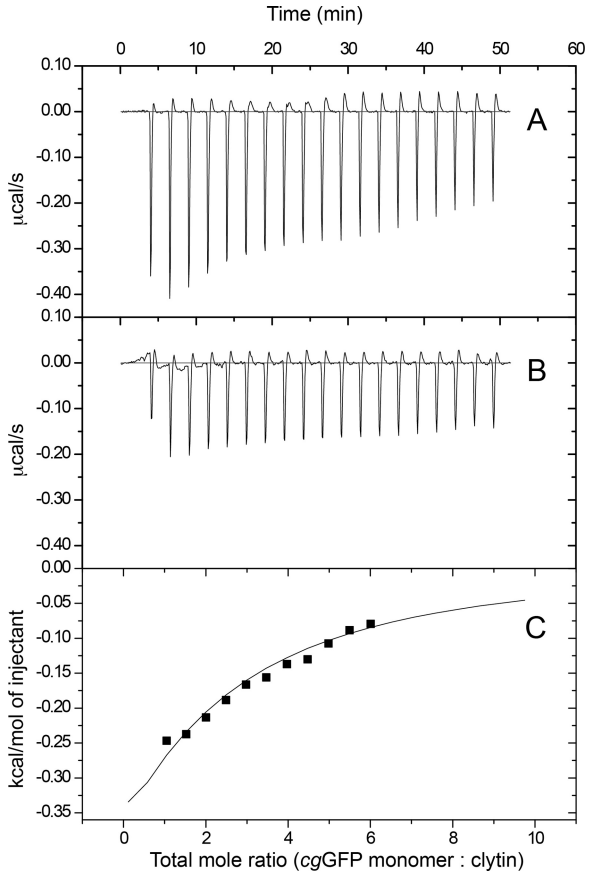

FIGURE 7. **ITC titration curves of clytin with *cg*GFP.** *A*, raw data of heat changes upon addition of *cg*GFP (4.68 mM monomer) into the cell containing 0.1 mM of clytin. *B*, corresponding heat of *cg*GFP dilution. *C*, processed data corresponding to the heat of each injection plotted against the molar ratio of total *cg*GFP to total clytin after subtraction of the heat of *cg*GFP dilution. Buffer contained 20 mM Tris-HCl, 10 mM NaCl, 2 mM EDTA, pH 7.0. The affinity constant (K_D = 0.90 ± 0.07 mM) was derived at 1:1 fixed stoichiometry.

nescence unit *in vitro*. There is a very favorable spectral overlap, 1.3×10^{-13} M^{-1} cm^3, between the bioluminescence from clytin, maximum 470 nm, and the absorption of *cg*GFP, having a monomer extinction coefficient of 64,000 M^{-1} cm^{-1} at 485 nm (4). Combined with the 45 Å separation of the donor and acceptor in the structure of the complex (Fig. 3), and the fact that the *cg*GFP will be dimerized in the complex, the electronic transitions are very strongly coupled. The energy from the bioluminescence reaction of the clytin will be quantitatively deposited into the excited state of the acceptor, the *cg*GFP. However, as the protein-protein complex is weak with a dissociation constant (K_{eq}) in the millimolar range according to the NMR chemical shift and ITC methods (Fig. 7), the mechanism by which added *cg*GFP at only micromolar concentrations is able to shift the bioluminescence toward the fluorescence of *cg*GFP, remains to be established.

The computational structure of the clytin-*cg*GFP complex resembles features of a weak protein-protein complex predominantly governed by electrostatic forces, with a low number of total intermolecular contacts (39–41). For a weak protein interaction the relatively high value of the clytin-*cg*GFP buried surface area (1,913 Å) derives from the impact of the distal (flexible) part of the clytin N terminus interacting with the top *cg*GFP barrel loops which together account for 30% of the total buried surface. However, intermolecular contacts in this region are minimal and the position of the clytin N terminus itself is highly variable among the best batch of structures, which implies a less significant impact of the distal part of the clytin N terminus compared with its proximal part and the α-helix D carrying the positive charge. This conclusion is supported by mutagenesis of clytin where we observe that deletion of the flexible part of the N terminus has the same effect on complex affinity and *cg*GFP color shift efficiency as the single substitutions K11A and K13A. These substitutions evidently affect electrostatics similarly to the high ionic strength conditions.

The question arises as to the physiological relevance of this clytin-*cg*GFP computational structure in Fig. 3. The photocytes of the jellyfish *Aequorea* and *Clytia* can be assumed to be the same, contain concentrations of the bioluminescence proteins estimated to be in the millimolar range (42, 47), similar to the concentrations required to form the complex detected by the NMR and ITC experiments. The *in vivo* bioluminescence spectra of several animals or their tissue samples, reveal nearly exact correspondence to the fluorescence of GFP, *i.e.* no contribution from the blue emission implying near 100% FRET efficiency (50, 52, 53). This demands that the origin of the emission is from a complex where the donor and acceptor have restricted separation and orientation. The inhibition of the GFP shift at increased salt concentration is consistent with electrostatic forces at the protein-protein interface driving the clytin-*cg*GFP complexation. This would argue against this same spatial structure existing *in vivo* if within the photocytes, the ionic strength approaches that of sea-water, or is even as low as that characteristic of eukaryotic cells, 100–150 mM because of potassium ions. On the other hand, several bioluminescent organisms are found to contain their bioluminescence systems within membrane enclosed vesicles, "lumisomes" in *Renilla* (54) and "scintillons" in the dinoflagellates (43). Such vesicles apparently modulate the intracellular environment for the benefit of the bioluminescence function (50). Because *cg*GFP itself is a tight dimer it is probable that *in vivo* the clytin-*cg*GFP complex is a heterotetramer. It should be noted that this supposition was advanced for *in vivo* aequorin-Aequorea GFP complex (51).

For a heterotetrameric complex of this size, >100 kDa, and weakly interacting, there is little prospect that further NMR experiments will yield unambiguous distance constraints for model refinement. Whether the spatial structure of the *in vivo* complex relates to that determined here at low ionic strength, hopefully will be proven by crystallography, although for a weak protein-protein complex this methodology presents its own set of impediments.

Acknowledgments—We thank Professor W. W. Ward (Rutgers University) for informative discussions of GFP interactions, and Professors Changwen Jin and Bin Xia (Beijing NMR Center, Peking University) for providing the 800 MHz NMR spectrometer facility.

REFERENCES

1. Shimomura, O. (2006) *Bioluminescence: Chemical Principles and Methods,* World Scientific, Singapore
2. Morin, J. G., and Hastings, J. W. (1971) *J. Cell Physiol.* **77,** 313–318
3. Ward, W. W., and Cormier, M. J. (1976) *J. Phys. Chem.* **80,** 2289–2291
4. Markova, S. V., Burakova, L. P., Frank, L. A., Golz, S., Korostileva, K. A., and Vysotski, E. S. (2010) *Photochem. Photobiol. Sci.* **9,** 757–765
5. McCoy, A. J., Grosse-Kunstleve, R. W., Adams, P. D., Winn, M. D., Storoni, L. C., and Read, R. J. (2007) *J. Appl. Crystallogr.* **40,** 658–674
6. Adams, P. D., Grosse-Kunstleve, R. W., Hung, L. W., Iorger, T. R., McCoy, A. J., Moriarty, N. W., Read, R. J., Sacchettini, J. C., Sauter, N. K., and Terwilliger, T. C. (2002) *Acta Crystallogr. Sect. D. Biol. Crystallogr.* **58,** 1948–1954
7. Emsley, P., and Cowtan, K. (2004) *Acta Crystallogr. Sect. D. Biol. Crystallogr.* **60,** 2126–2132
8. Davis, I. W., Leaver-Fay, A., Chen, V. B., Block, J. N., Kapral, G. J., Wang, X., Murray, L. W., Arendall, W. B., 3rd, Snoeyink, J., Richardson, J. S., and Richardson, D. C. (2007) *Nucleic Acids Res.* **35,** W375–W383
9. Vagin, A. A., and Isupov, M. N. (1997) *J. Appl. Crystallogr.* **30,** 1022–1025
10. McRee, D. E. (1999) *J. Struct. Biol.* **125,** 156–165
11. Murshudov, G. N., Vagin, A. A., and Dodson, E. J. (1997) *Acta Crystallogr. Sect. D. Biol. Crystallogr.* **53,** 240–255
12. Bradford, M. M. (1976) *Anal. Biochem.* **72,** 248–254
13. Johnson, B. A., and Blevins, R. A. (1994) *J. Biomol. NMR* **4,** 603–614
14. Jung, Y. S., and Zweckstetter, M. (2004) *J. Biomol. NMR* **30,** 11–23
15. Sattler, M., Schleucher, J., and Griesinger, C. (1999) *Prog. NMR Spectrosc.* **34,** 93–158
16. Xu, Y., Zheng, Y., Fan, J. S., and Yang, D. (2006) *Nat. Methods* **3,** 931–937
17. Dominguez, C., Boelens, R., and Bonvin, A. M. (2003) *J. Am. Chem. Soc.* **125,** 1731–1737
18. de Vries, S. J., van Dijk, A. D., Krzeminski, M., van Dijk, M., Thureau, A., Hsu, V., Wassenaar, T., and Bonvin, A. M. (2007) *Proteins: Struct., Funct., Bioinf.* **69,** 726–733
19. Brünger, A. T., Adams, P. D., Clore, G. M., DeLano, W. L., Gros, P., Grosse-Kunstleve, R. W., Jiang, J. S., Kuszewski, J., Nilges, M., Pannu, N. S., Read, R. J., Rice, L. M., Simonson, T., and Warren, G. L. (1998) *Acta Crystallogr. Sect. D. Biol. Crystallogr.* **54,** 905–921
20. Liu, Z. J., Vysotski, E. S., Chen, C. J., Rose, J. P., Lee, J., and Wang, B. C. (2000) *Protein Sci.* **9,** 2085–2093
21. Head, J. F., Inouye, S., Teranishi, K., and Shimomura, O. (2000) *Nature* **405,** 372–376
22. Vysotski, E. S., and Lee, J. (2004) *Acc. Chem. Res.* **37,** 405–415
23. Liu, Z. J., Vysotski, E. S., Deng, L., Lee, J., Rose, J., and Wang, B. C. (2003) *Biochem. Biophys. Res. Commun.* **311,** 433–439
24. Remington, S. J. (2006) *Curr. Opin. Struct. Biol.* **16,** 714–721
25. Wachter, R. M. (2006) *Photochem. Photobiol.* **82,** 339–344
26. Ormö, M., Cubitt, A. B., Kallio, K., Gross, L. A., Tsien, R. Y., and Remington, S. J. (1996) *Science* **273,** 1392–1395
27. Loening, A. M., Fenn, T. D., and Gambhir, S. S. (2007) *J. Mol. Biol.* **374,** 1017–1028
28. Levine, L. D., and Ward, W. W. (1982) *Comp. Biochem. Physiol., Part B: Comp. Biochem.* **72,** 77–85
29. Ward, W. W. (1998) in *Green Fluorescent Protein* (Chalfie, M., and Kain, S., eds), pp. 45–75, Wiley-Liss, New York
30. Ohashi, W., Inouye, S., Yamazaki, T., Doi-Katayama, Y., Yokoyama, S., and Hirota, H. (2005) *J. Biomol. NMR* **31,** 375–376
31. Nicastro, G., Menon, R. P., Masino, L., Knowles, P. P., McDonald, N. Q., and Pastore, A. (2005) *Proc. Natl. Acad. Sci. U.S.A.* **102,** 10493–10498
32. Zhang, N., Liu, L., Liu, F., Wagner, C. R., Hanna, P. E., and Walters, K. J. (2006) *J. Mol. Biol.* **363,** 188–200
33. Koglin, A., Mofid, M. R., Löhr, F., Schäfer, B., Rogov, V. V., Blum, M. M., Mittag, T., Marahiel, M. A., Bernhard, F., and Dötsch, V. (2006) *Science* **312,** 273–276
34. Schreiner, P., Chen, X., Husnjak, K., Randles, L., Zhang, N., Elsasser, S., Finley, D., Dikic, I., Walters, K. J., and Groll, M. (2008) *Nature* **453,** 548–552
35. Yuan, X., Simpson, P., McKeown, C., Kondo, H., Uchiyama, K., Wallis, R., Dreveny, I., Keetch, C., Zhang, X., Robinson, C., Freemont, P., and Matthews, S. (2004) *EMBO J.* **23,** 1463–1473
36. Card, P. B., Erbel, P. J., and Gardner, K. H. (2005) *J. Mol. Biol.* **353,** 664–677
37. Banci, L., Bertini, I., Ciofi-Baffoni, S., Kandias, N. G., Robinson, N. J., Spyroulias, G. A., Su, X. C., Tottey, S., and Vanarotti, M. (2006) *Proc. Natl. Acad. Sci. U.S.A.* **103,** 8320–8325
38. Lo Conte, L., Chothia, C., and Janin, J. (1999) *J. Mol. Biol.* **285,** 2177–2198
39. Reichmann, D., Rahat, O., Cohen, M., Neuvirth, H., and Schreiber, G. (2007) *Curr. Opin. Struct. Biol.* **17,** 67–76
40. Prudêncio, M., and Ubbink, M. (2004) *J. Mol. Recognit.* **17,** 524–539
41. Kiel, C., Selzer, T., Shaul, Y., Schreiber, G., and Herrmann, C. (2004) *Proc. Natl. Acad. Sci. U.S.A.* **101,** 9223–9228
42. Morise, H., Shimomura, O., Johnson, F. H., and Winant, J. (1974) *Biochemistry* **13,** 2656–2662
43. Nicolas, M. T., Nicolas, G., Johnson, C. H., Bassot, J. M., and Hastings, J. W. (1987) *J. Cell Biol.* **105,** 723–735
44. Ward, W. W., and Cormier, M. J. (1978) *Photochem. Photobiol.* **27,** 389–396
45. Ward, W. W., and Cormier, M. J. (1978) *Methods Enzymol.* **57,** 257–267
46. Ward, W. W., and Cormier, M. J. (1979) *J. Biol. Chem.* **254,** 781–788
47. Cutler, M. W. (1995) *Ph.D. Thesis*, Rutgers University, New Brunswick, NJ
48. Deleted in proof
49. Deleted in proof
50. Morin, J. G., and Hastings, J. W. (1971) *J. Cell Physiol.* **77,** 313–318
51. Cutler, M. W., and Ward, W. W. (1997) in *Bioluminescence and Chemiluminescence: Molecular Reporting with Photons* (Hastings, J. W., Kricka, L. J., and Stanley, P. E., eds), pp. 596–599, Wiley-Liss, New York
52. Wampler, J. E., Hori, K., Lee, J. W., and Cormier, M. J. (1971) *Biochemistry* **10,** 2903–2909
53. Wampler, J. E., Karkhanis, Y. D., Morin, J. G., and Cormier, M. J. (1973) *Biochim. Biophys. Acta* **314,** 104–109
54. Anderson, J. M., and Cormier, M. J. (1973) *J. Biol. Chem.* **248,** 2937–2943
55. Dolinsky, T. J., Nielsen, J. E., McCammon, J. A., and Baker, N. A. (2004) *Nucleic Acids Res.* **32,** W665–W667
56. Baker, N. A., Sept, D., Joseph, S., Holst, M. J., and McCammon, J. A. (2001) *Proc. Natl. Acad. Sci. U.S.A.* **98,** 10037–10041
57. Turnbull, W. B., and Daranas, A. H. (2003) *J. Am. Chem. Soc.* **125,** 14859–14866